





# Ionic liquid coating for charge mitigation of solar modules in space: Electron microscopy on insulating nanosphere lithography patterned surfaces

Mirco Wendt<sup>1,3,4</sup> , Franziska Dorn<sup>1,3</sup>, Regina Lange<sup>1,3</sup>, Ralf Ludwig<sup>2,3</sup> , Jens Berdermann<sup>4</sup> , Ingo Barke<sup>1,3</sup>, and Sylvia Speller<sup>1,3,\*</sup> 

<sup>1</sup> Institute of Physics, University of Rostock, Albert-Einstein-Straße 23, 18059 Rostock, Germany

<sup>2</sup> Institute of Chemistry, University of Rostock, Albert-Einstein-Straße 3a, 18059 Rostock, Germany

<sup>3</sup> Department of Life, Light & Matter, University of Rostock, Albert-Einstein-Straße 21, 18059 Rostock, Germany

<sup>4</sup> German Aerospace Center, Institute for Solar-Terrestrial Physics, Kalkhorstweg 53, 17235 Neustrelitz, Germany

Received 28 September 2023 / Accepted 24 May 2024

**Abstract**—Surfaces of satellites and spacecraft are exposed to high energy charged particles from the solar wind, especially during space weather events. This can lead to differential charging, which is a common reason for hardware degradation and sensor errors. Solutions like coatings are required to avoid excessive cost and weight. Mimicking the electron part of space-like environments in ultra-high vacuum (UHV) chambers can be achieved by using electrons emitted by a scanning electron microscope (SEM). As a performance test for the discharge capabilities we use the quality of electron microscopy images on otherwise insulating substrates such as glass, structured by nanosphere lithography and coated with an ionic liquid (IL). Additionally, the surface potential was measured by Kelvin Probe Force Spectroscopy. The IL film (BMP DCA) was applied ex-situ and a thickness of 12.8 ( $\pm 0.8$ ) nm was determined by reflectometry and confirmed by dynamic atomic force microscopy. Such a film of ionic liquid would lead to an additional mass of below 20 mg and negligible additional material costs. The light absorption and influence of ionic liquid coatings on the current output of an actual solar cell were investigated. The results indicate, that these coatings are promising candidates for surface charge mitigation with a high potential for application.

**Keywords:** Conductive coating / Charging mitigation / Ionic liquid / Solar panel / Satellite / Surface charges / Spacecrafts

## 1 Introduction

A number of solar storms have led to malfunctions or damage of infrastructure in space and even on Earth via charging and uncontrolled voltage buildup (Lu et al., 2019; Bonin et al., 2010). Satellite anomalies have been recorded at geosynchronous orbit altitudes (Choi et al., 2011). Especially beyond 10,000 km altitude or at high inclinations ( $\pm 50$  degree latitude), a high differential surface charging hazard is experienced leading to potential differences of several thousands of Volt across various parts of a satellite (Garrett and Whittlesey, 2012). This includes the geosynchronous orbit for which SCATHA and ATS missions reported electron current densities of  $6 \times 10^{12}$  e/(m<sup>2</sup>s) in average and  $1.66 \times 10^{13}$  e/(m<sup>2</sup>s) under storm conditions and average ion current densities of

$3 \times 10^{11}$  e/(m<sup>2</sup>s) (Garrett and Whittlesey, 2012). The magnitude, sign, and dynamics of the total charging of a conducting spacecraft have been studied by data taken on the Van Allen Probes in geosynchronous orbit altitudes, positive as well as negative charging, the latter up to 1000 V, has been detected (Sarno-Smith et al., 2016). Also, at low earth orbit, though considered less invasive, occasional or periodic charging through high energy electrons has been reported (Anderson, 2012).

As solar cell cover glasses as insulating parts are most affected, the requirements for film mitigating charging involve high optical transparency in the photovoltaically absorbable band (i.e. 375–850 nm) while maintaining decent electrical conductivity in order to balance the above-mentioned current densities. Secondary parameters are low-weight (i.e. thin films) and ease of application to achieve low costs, as large areas have to be coated. Materials fulfilling these requirements are rare, as good

\*Corresponding author: [sylvia.speller@uni-rostock.de](mailto:sylvia.speller@uni-rostock.de)

electron conductors, due to only small or absent band gaps, usually are opaque.

Thus, various existing mitigation strategies come with their own sets of drawbacks. A common practice is to accept surface charging and design spacecraft components accordingly, so they may withstand these conditions. However, such approaches require significant computational work (Vostrikov and Prokofeva, 2022). To avoid discharges, minimum distances between solar modules can be increased leading to greater mass and size. Counter-charging via ion sources is possible but hard to apply homogeneously, and over longer periods of time they can damage the surface.

Another approach is the application of conductive surface coatings. Coating solar cells with indium tin oxide is costly and even if an additional anti-reflection coating is applied, spectral power losses are in the range of 2–3% for a 100 nm thick film, (Biyikli et al., 2004) and would subsequently lead to lower solar cell power output. Conductive polymers such as Poly-3,4-ethylenedioxythiophene (PEDOT) are sufficiently conductive, yet show significant light absorption, even in ultra-thin films (Singh and Kumar, 2019; Kim et al., 2011), disqualifying them from being considered for applications as protective coatings for solar cells. Also, they may degrade under long-term UV radiation.

Ionic liquids (IL), salts with melting points below room temperature, have already proven themselves as conductive coating materials in electron microscopy, especially for either very rough and/or wet biological samples (Arimoto et al., 2008; Tsuda et al., 2011). Their vapour pressure is almost negligible (Ravula et al., 2019), thus they are stable under vacuum conditions. Additionally, they are also inexpensive, easy to apply and mostly transparent. In this work, we address, whether ionic liquids can function as a conductive molecular film for flat insulator surfaces such as the cover glasses of solar cells in the context of space applications.

We mimic the electron radiation of space-like environments using the electron beam of a scanning electron microscope. We assess charge mitigation performance by means of SEM imaging performance, i.e. good contrast of a test structure and absence of typical charging features. In addition we used Kelvin probe force spectroscopy to quantify residual charges in terms of surface potentials. Experiments were performed at atmospheric pressure, high vacuum and ultra-high vacuum to demonstrate stability over a wide range of pressures. The thickness of the coating was determined by reflectometry and validated using atomic force microscopy. Absorption measurements in the visible range and short circuit currents of coated and untreated commercially available solar cells do not suggest noticeable light absorption and hence we expect little if any effects on the power output.

## 2 Sample preparation

As test samples, we used glass coverslips (Menzel). These were UV-ozone treated for approximately one hour in order to increase hydrophilicity, before further preparation. To generate nanoscopic structures on these otherwise unstructured samples, we utilized nanosphere lithography, first introduced

by Fischer and Zingsheim (1981). These serve as reference structures on the samples in subsequent AFM and SEM measurements but are not required to form the conductive layer proposed in this work. We created a 1:1 solution of the as-provided polystyrene spheres (diameters 0.1, 0.3, 1.0 or 3.0  $\mu\text{m}$ , Microparticles GmbH, Germany) dispersion (10% w/v) and ethanol. Drop-casting 5  $\mu\text{L}$  of this solution on the substrates resulted in self-assembly and subsequent formation of monolayers of hexagonally-packed arrays exhibiting triangular voids between the spheres. This includes occasional defects such as domain boundaries and free areas. A  $\sim 30$  nm thick film of Au (purity 99.999%) was evaporated on the polystyrene spheres (PS) in a BOC Edwards Auto 500 thin film coating system in thermal evaporation mode at a pressure of around  $5 \times 10^{-4}$  Pa. No adhesion promoter has been used. The film thickness was monitored in situ by a quartz micro-balance. Both structures, sphere mask and Au islands, and the film thickness have been checked by force microscopy (Park XE-100) under ambient conditions. The polystyrene spheres were dissolved using tetrahydrofuran (THF) in an ultrasonic bath for 25 s. Varying the diameters of the spheres used, triangle edge lengths of 1.5  $\mu\text{m}$  to 150 nm can be achieved, depending on the sphere diameter used and the position of the sample and gold source relative to each other inside the coating system.

After removing the spheres, residual material may be left at the sphere positions, presumably originating from the PS dispersion. To remove those, the sample was again UV-ozone treated (PSD series, Novascan) for 90 min.

The IL coating is applied by drop-casting a solution of 3% 1-Butyl-1-methylpyrrolidinium dicyanamide (BMP DCA, Iolitec) in deionized water onto the coverslip, which has been UV-ozone treated again ( $\sim 90$  min), to increase hydrophilicity. The excess liquid was removed by wiping the sample with a cloth after which it was left to dry in air (Fig. 1).

## 3 Coating thickness

The film thickness was determined using a commercial reflectometer (NanoCalc-XR, Ocean Optics) by placing a sample on a silicon wafer and irradiating it using a deuterium lamp. The intensity of the reflected light depending on the wavelength was measured. Fitting the acquired spectrum using a model of a stacked system of (from top to bottom) BMP DCA ( $n = 1.5$ ; González et al., 2012), glass ( $n = 1.46$ ; Aspnes and Studna, 1983) and silicon ( $n = 3.98$ ; Malitson, 1965) yielded a film thickness of  $12.8 \pm 0.8$  nm corresponding to an increased mass per area of  $15 \text{ mg/m}^2$ .

To investigate whether the IL forms a continuous layer, we carried out AFM measurements in ambient, comparing a glass sample with gold nanotriangles to a sample with gold nanotriangles and a BMP DCA coating. Topographies acquired using a “non-contact” silicon cantilever (SSS-NCHR, Nanosensors) are shown in Figure 2.

The uncoated gold structures (Fig. 2, left) appear to be  $\sim 25$  nm high, which is in agreement with the target thickness of the gold film during evaporation. The image clearly shows triangles with sharp edges of slightly varying lengths. Where the polystyrene spheres have been located prior to removal,

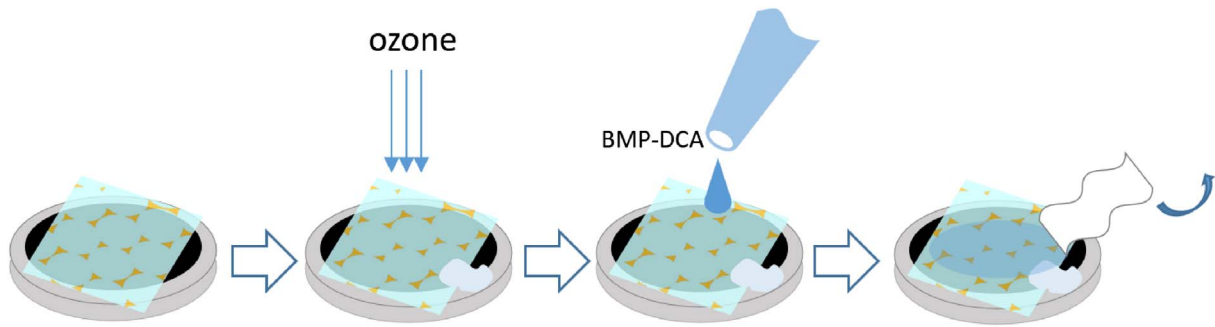


**Figure 1.** Scheme of preparation of the IL layer.

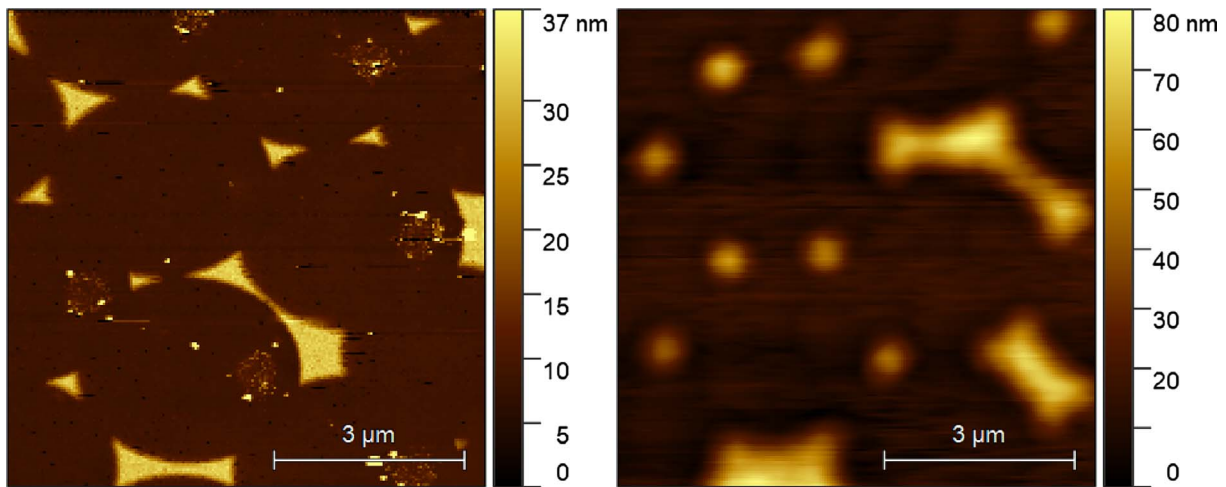


**Figure 2.** AFM topography images of gold nanostructures prepared by nanosphere lithography (using 3  $\mu\text{m}$  spheres as mask) without (left) and with (right) a coating of BMP DCA. Changes in resolution and apparent heights of the gold triangles are clearly visible.

some residual material is visible, despite the additional UV-ozone treatment. This indicates, that it is some inorganic material, yet its origin is unknown.

The topography image acquired on the coated sample (Fig. 2, right) shows gold structures as well, yet they generally lack triangular shape and do not exhibit as pronounced edges as was previously the case. We attribute this to the layer of BMP DCA on top, which would smooth out such edges by forming menisci to minimize surface energy. The oscillation frequency of  $\sim 350$  kHz of the cantilever should repress the periodic formation of a meniscus of liquid between tip and samples (Santos and Verdaguer, 2016), an effect that may also be supported by repulsive interaction between tip and liquid due to the tip's low hydrophilicity. Thus, we believe that the surface of the ionic liquid film was imaged. This is in accordance with the increase in height of the gold structure up to 60 nm with respect to the substrate. Due to the higher hydrophilicity of the gold compared to the glass substrate, droplets may form around the triangles. This, on the other hand, indicates a rather thin film left on the glass, especially as the broader shape and distribution of the gold structures can still be identified. As the above-mentioned residue visible on the uncoated sample can no longer be observed, possibly the layer is still thick enough to encapsulate it, if it was not removed by the application of the coating already,

e.g. by successive wiping of the sample. In view of these results, the thickness determined by reflectometry seems plausible. Moreover, due to the absence of gold structures of solar cell cover glasses, thickness inhomogeneities in the ionic liquid layer on the scale observed should not occur.

AFM measurements can of course only cover a very limited surface area. Regarding the homogeneity of the IL film on larger scales, the evaluation of SEM images such as depicted in Figure 3 is more useful. Uncoated areas would yield distinct charging signatures of the exposed glass while areas of increased coating thickness would be darker in SEM images, due to a decrease in detected secondary electrons. We did, however, not observe such behaviour in our SEM observations, which indicates that the film is in fact homogeneous. Furthermore, we did not observe changes in BMP DCA coatings homogeneity over the course of several months for the UHV stored sample, suggesting sufficient stability for applications. Additionally, using the thickness information given, based on sputter yield coefficient considerations (Schmid, 2023), we estimate with an ion current density of  $3 \times 10^{11}$  e/(m<sup>2</sup>s) (Garrett and Whittlesey, 2012) it would take several hundred years for the BMP DCA layer to be eroded by proton sputtering. As the solution applied to create the IL film already consisted of 97% water, we regard additional water intake due to the hygroscopic nature

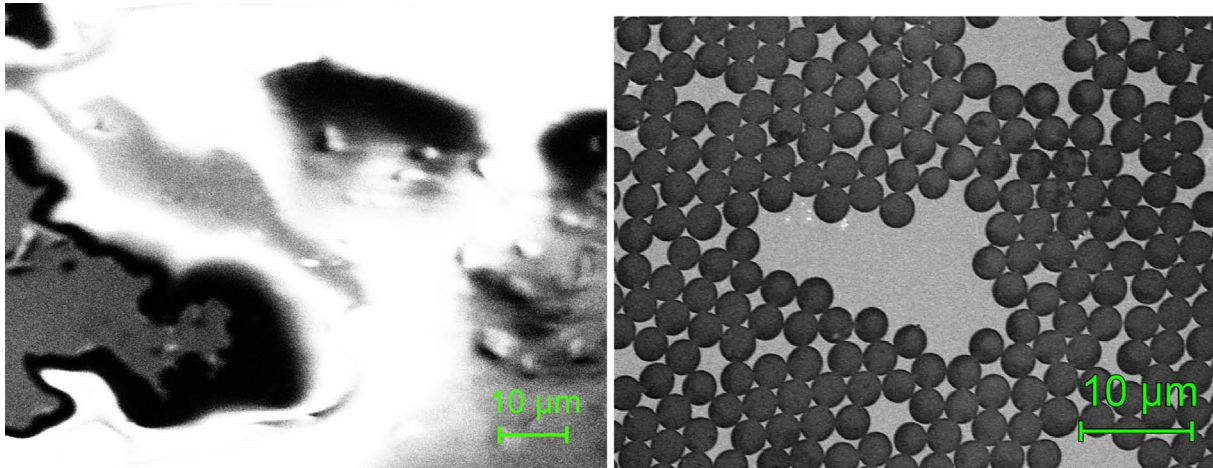


**Figure 3.** Left: SEM image of bare glass with gold nanostructures prepared by nanosphere lithography (using 3  $\mu\text{m}$  spheres as mask), 5 keV,  $1.5 \times 10^{18} \text{ e/m}^2$ . The metal nanostructures are hardly visible due to excessive charging (compare right). Right: Same sample type as left, but now coated with BMP DCA, 5 keV,  $1.8 \times 10^{18} \text{ e/m}^2$ . The metal nanostructures are clearly resolved.

of IL, i.e. during ground storage, to be negligible. For samples stored at ambient conditions, IL films were also stable at least for days.

#### 4 Imaging in SEM

To assess the general performance of the IL films, measurements were performed in a conventional electron microscope (EVO MA 10 SEM, Zeiss). The vacuum in the chamber was in the regime of  $10^{-4}$  Pa. Primary energies of the electrons were varied from 5 keV to 25 keV, though the images shown in Figure 3 were both acquired at 5 keV primary electron energy. The beam current was in the range of  $\sim 100$  pA. When scanning over an image of  $100 \mu\text{m}^2$ , this results in effective current densities of  $1 \text{ A/m}^2 \approx 6.2 \times 10^{18} \text{ e/(m}^2\text{s)}$ , which is approximately six orders of magnitude higher than the aforementioned current densities in space.

Conductive Ag lacquer was applied to the sample surface prior to IL coating to establish an electric connection between the glass slide and the SEM sample holder, to which the samples were glued by a conductive carbon pad.

In Figure 3 a comparison between two differently treated glass samples is depicted. The image on the left was obtained from a glass sample with gold nanotriangles, whereas the image on the right shows the same type of sample with an additional coating of BMP DCA. Both samples were subjected to the same aforementioned pressure and beam current. The uncoated sample was imaged at low magnification i.e. at a lower equivalent current density of  $6 \times 10^{16} \text{ e/(m}^2\text{s)}$ . No clear image of the surface could be acquired. The dominating feature is a bright region, essentially spanning across the entire picture. Such regions are typical indicators of sample charging. Electrons accumulate on the surface and their fields interfere with the primary electrons, reflecting them towards the detector (Shaffner and Veld, 1971). The dark fringes seen around such heavily charged regions are also a result of the electric fields on the sample surface, as secondary electrons emitted there are guided away by lateral fields (Cazaux, 2004). On the left

side of the image, a grey area can be seen. This could be a gold island, where no polystyrene spheres had assembled. This island continues out of the image frame. As the gold layer is conductive, even though at a floating potential, the accumulated charge would remain at a lower density, enabling at least temporary imaging of that specific region.

On the coated sample (right), the triangles and larger gold islands produced by the nanosphere lithography can be observed, as they appear brighter than the underlying glass. This is a result of higher electron density and thus interaction cross-section of gold compared to silicon and oxygen, hence increasing secondary electron yield. As 3  $\mu\text{m}$  polystyrene spheres were used for the assembly, the edges of the triangles show edge lengths of below 1.5  $\mu\text{m}$ . Contrary to the AFM measurements discussed earlier, in this image the triangles still have sharp edges and tips, supporting our explanation that previously (Fig. 2 right) the surface of the liquid has been imaged. For the electron beam, however, such a thin ionic liquid film should be more or less transparent, since it is mainly comprised of light elements at low density so that the electrons mainly interact with underlying materials.

Figure 4 shows an SEM image of a BMP DCA-treated glass sample with gold nanostructures prepared by nanosphere lithography using 300 nm spheres as a mask. Again, the gold structures appear brighter than the underlying substrate. Due to the smaller PS spheres used, triangle edge lengths are below 150 nm. Domain boundaries are also visible, as well as a region at the top left, in which the substrate appears brighter than in the rest of the image. This likely corresponds to the onset of surface charging, similar to what was observed in Figure 3 left, although in this case much weaker. We attribute this to inhomogeneities in the BMP DCA film: it might be thinner in that particular region and therefore exhibits a lower conductivity. As the magnification for this image was higher than in the previous ones, so was the effective current density and also the total electron density of  $1.8 \times 10^{20} \text{ e/m}^2$ . This is two orders of magnitude more than in the previous images and roughly represents the amount of charges, a solar panel in space would be exposed to over the course of an entire year, assuming average conditions.

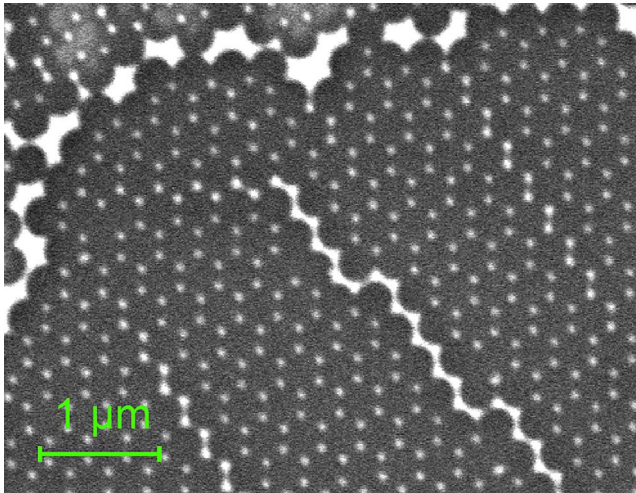


**Figure 4.** SEM image of BMP DCA treated glass with gold nanostructures prepared by nanosphere lithography (using 300 nm spheres as mask), 5 keV,  $1.8 \times 10^{20} \text{ e/m}^2$ .

As the exposure in our device only takes seconds, it is possible that in actual space environments, no noticeable charging would occur. At longer time scales distribution processes such as diffusion across the surface, both of the ions as well as the electrons, could lead to a decrease in the total surface potential. Additionally, exposure to direct sunlight might resolve such charge accumulations by the emission of photoelectrons. On the other hand, although experiments were performed at primary energies of 5 keV, which should be higher than a significant portion of the electron spectrum in space, electrons with even higher energies might lead to the generation of ions buried inside the glass. These can, of course, not be mitigated by coating the surface. Furthermore, performance decrease due to damage by ionizing radiation has not been considered.

Ultimately, to make predictions regarding the long-term behavior of such a coating, it will be important, to better understand the underlying mechanism preventing the build-up of surface charges. Apart from a simple model of electrons hopping from one ion to another, we can not rule out other processes such as chemical reactions taking place in the IL (ultimately leading to a finite amount of charges that can be captured, depending on the IL layer thickness) or a supercapacitor-like behaviour, in which the IL effectively shields the surface charges (by extension such a behaviour would indeed also shield the potential generated by buried ions).

## 5 Surface potential measurements

As the SEM images only yielded qualitative information, we measured the surface potential of our sample by Kelvin Probe Force Spectroscopy (KPFs). To this end, we used a DuoProbe UHV-VT-SPM system by RHK, coupled with a UHV-SEM (Orsay Eclipse+). The base pressure in this instrument is  $2 \times 10^{-8} \text{ Pa}$ , which also better mimics conditions in space. The KPFs measurements were performed utilizing quartz

tuning forks with a Pt/Ir wire as a tip attached to one prong. This method was introduced by [Giessibl and Trafas \(1994\)](#).

In short, the shift of the eigenfrequency of the tuning fork is measured when the tip is close to the surface. This shift is due to interaction forces (e.g. van der Waals forces or Coulomb forces due to charges on the surface) between the metal tip and the surface. For KPFs, a voltage is applied to the sample to compensate for the surface potential. If this is achieved, the forces between tip and sample are minimized. The dependence of the frequency shift on the potential difference, and hence on the voltage, is parabolic. By determining the voltage required for compensation, one can therefore also determine the surface potential, which, in this case, can directly be attributed to the presence of charges on the surface.

In [Figure 5](#) the results of such a surface potential measurement for glass with gold nanostructures (red) and glass with gold nanostructures and BMP DCA coating (blue) after exposure to  $\sim 10^{17} \text{ e/m}^2$  each are depicted. The measured frequency shift is plotted versus applied voltage. The data for untreated glass was obtained at negative frequency shift, as in this scenario attractive electrostatic forces are dominant (at least as long as tip and sample are not in contact). This also means compensating the surface potential actually maximises the frequency shift. At the maximum of the parabolic curve is clearly shifted towards a positive voltage. Requiring a positive voltage for compensation means the actual potential of the surface is negative, which is what one would expect for a negatively charged surface. Using a parabolic fit function, we find the minimal frequency shift to be at 97 V bias voltage, i.e., the surface potential is  $-97 \text{ V}$ . Considering, that for total reflection of the primary electrons potentials similar to their primary energy are required ([Belhaj et al., 2006](#)), the measured potential is rather low. This points to partial charge depletion after deposition.

In order to estimate the residing charge density, a simple electrostatic model can be employed. Assuming the charges on the glass (thickness: 0.15 mm, relative dielectric constant: 4.6) form a capacitor with the metallic sample holder, such potentials would correspond to charge densities of approximately  $10^{14} \text{ e/m}^2$ , disregarding the vicinity of the tip. This is far lower than what the sample was exposed to. However, this is expected, as the secondary electrons reduce the net charge residing at the surface. Additionally, the initial charge directly after exposure is likely larger than at the time of potential measurements because of ongoing discharging processes. In fact, repeating this measurement several times yielded consistently decreasing surface potentials, until after one day a stable surface potential of  $-33.6 \text{ V}$  was reached. This indicates that, although experiments were conducted in UHV environments, some residual discharging channels remained. This may be due to the native hydration layer of the glass sample, as it has not been heated in the chamber. Another decay channel may be due to the tip of the AFM itself, since its distance to the sample surface is low, potentially enabling tunnelling transport or even intermittent contact. As a result, quantitative information on the actual surface charge density after electron exposure is hard to obtain from this method.

For the coated sample, the same procedure suggests  $+0.08 \text{ V}$  bias voltage for full surface potential compensation and thus a surface potential of  $-0.08 \text{ V}$ . (Before electron exposure surface potentials of  $0.3 \text{ V}$  were observed). Such small surface poten-

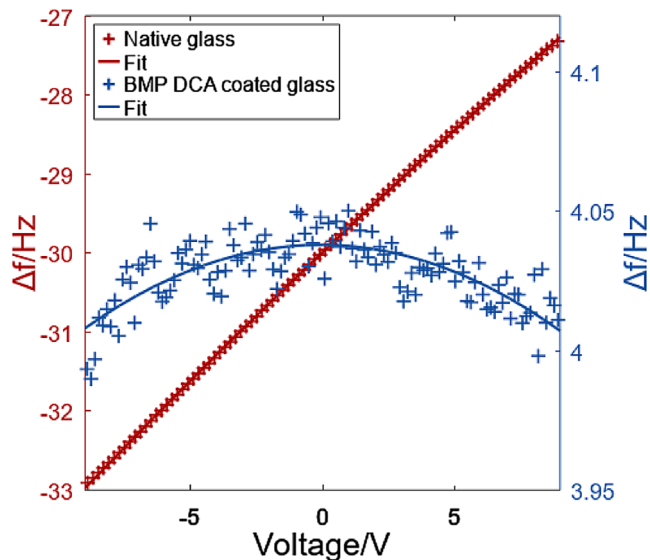


**Figure 5.** df-V-spectroscopy curves for glass with gold nanostructures (red) and glass with gold nanostructures and BMP DCA coating (blue) after exposure to  $\sim 10^{17}$  e/m<sup>2</sup> each. Tip material: Pt/Ir. Crosses indicate experimental data, continuous lines the parabolic least-square fits. Red fit:  $-0.00016 \text{ Hz/V}^2 \times (V - 97 \text{ V})^2 - 15 \text{ Hz}$ ; blue fit:  $-0.00037 \text{ Hz/V}^2 \times (V - 0.08 \text{ V})^2 + 4 \text{ Hz}$ .

tials are usually not the result of charges on the surface, but rather from the contact potential difference between tip and sample (Sadewasser and Glatzel, 2012). Note that in this measurement, we chose the frequency shift to be positive, in contrast to the previous example (Native glass  $-15$  Hz, coated glass  $+4$  Hz). The change in sign corresponds to the dominance of repulsive interaction, e.g. Pauli repulsion. This choice has practical reasons: while for charged surfaces long range Coulomb interaction makes it easy to approach in the attractive regime, thus avoiding tip-sample contact, for uncharged surfaces, such attractive interactions are limited to short ranged van-der-Waals forces. This makes it significantly easier to approach in the repulsive regime. However, for evaluation, this does not make a difference but only adds a constant offset to the curves. Based on such tuning-fork frequency shifts, a more precise assessment of charges at surfaces after exposure to electrons may be achieved by taking into account the localised charge upon localized electron exposure in conjunction with effects due to the vicinity of the tip (Orihuea et al., 2016). Observing the charge density evolution in time and space would be a promising approach for identifying conduction mechanisms for IL.

## 6 Light absorption of the BMP DCA coating

Having demonstrated the ability of thin ionic liquid films to mitigate surface charging, the question remains, whether such a coating is expected to impact the power output of solar cells, especially by additional light absorption in the IL layer. To address this, we measured the absorbance of a BMP DCA film on glass, prepared according to the same procedure as before. This time, no gold nanostructures were prepared to

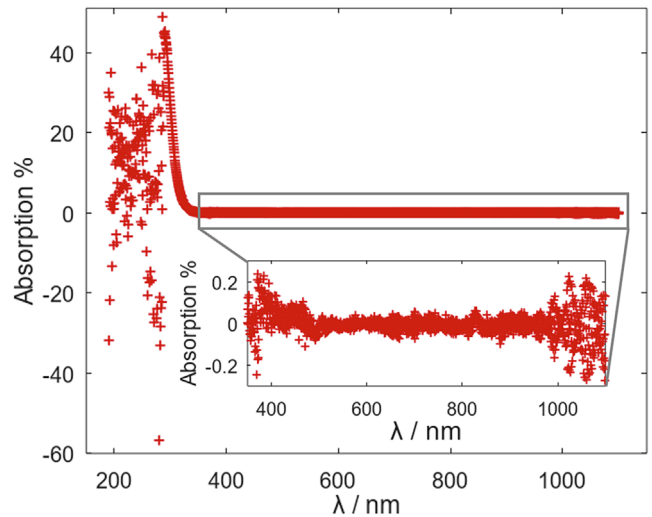


**Figure 6.** Absorption for a BMP DCA layer on borosilicate glass at different wavelengths.

avoid interference with the BMP DCA absorption signal. Absorbance Spectroscopy was carried out in a commercial device (Specord 50, Analytik Jena) using a white light source. As a reference sample, we used a UV-Ozone cleaned glass cover slide to acquire only the absorbance related to the addition of BMP DCA.

According to the Beer-Lambert law, a relative absorption in % can be calculated from this, indicating the fraction of light absorbed by the introduction of the BMP DCA coating. The results are shown in Figure 6. Above 350 nm the absorption is 0.2% or lower, while for lower wavelengths strong variations due to the onset of absorption of the borosilicate glass, and thus low values of detected photons are observed.

The absorption shown for wavelengths greater than 350 nm is in the range of the device's measurement uncertainty, suggesting negligible absorption of the IL film. In any case, light absorption is significantly lower than the typical 2–3% absorption of 100 nm thick films of indium tin oxide (Biyikli et al., 2004).

These findings are in agreement with measurements of short circuit currents shown in the Supplementary material: for a given illuminance, the current only decreases in the range of 1–3%, with uncertainty in the same range.

We thus do not expect the proposed coating to affect the power output of solar cells, yet dedicated testing of this would be advisable.

## 7 Conclusion & outlook

We have presented a procedure to generate nanoscopic surface coatings using ionic liquids such as BMP DCA. AFM and reflectometry measurements verified that the thickness of such conductive coatings is in the range of a few tens of nanometers. By imaging gold nanotriangles on insulating substrates in SEM, we showed that the coating is sufficiently conductive to compensate for effective current densities far exceeding average

conditions in space. Additional measurements of the surface potential of BMP DCA coated glass compared to uncoated samples confirmed that no residual surface charges accumulate. As the layers were exposed to rather harsh conditions, we expect that they should be well suited for mitigation of surface charges in actual space environments.

Additionally, we have found that our BMP DCA shows no distinct absorption in the visible range, which is consistent with our observation that solar cells coated with BMP DCA produce only slightly reduced short circuit currents compared to uncoated cells. The absorption is also lower than that of indium tin oxide, all while being far less expensive than the latter.

Both electrical and optical properties could, of course, also undergo detrimental changes when exposed to ionizing radiation for longer periods of time. This potential degradation requires further studies. Although we do not regard the sputtering of the film by highly energetic protons to be problematic, how the layer in general reacts to the exposure with ions will be studied in a later step.

Furthermore, as the conduction mechanisms in ionic liquids are rather poorly understood, we think time and spatially resolved Kelvin Probe Force Spectroscopy measurements could yield valuable insights.

To definitively assess its performance, testing ionic liquid coatings in actual space environments will be a necessary step.

## Acknowledgements

We would like to thank Franziska Fennel and Stefan Lochbruchner for the absorbance measurements, Christian Imhof for fruitful discussion and Norbert Steinfeldt for the opportunity to use the solar simulation lamp. The editor thanks Sebastian Grau, Miroslaw Chorazewski and an anonymous reviewer for their assistance in evaluating this paper.

## Funding

Funding by the Deutsche Forschungsgemeinschaft (DFG, German Research Foundation) within project number INST 264/110-1 FUGG, SFB 1477 “Light-Matter Interactions at Interfaces”, project number 441234705, SFB 1270 “Electrically Active Implants”, project number 299150580 and Priority Programme SPP 1807 “Control of Dispersion Interactions in Molecular Chemistry”, project number 269854963, is acknowledged.

## Supplementary material

The supplementary material of this article is available at <https://www.swsc-journal.org/10.1051/swsc/2024019/olm>.

Ionic liquid coating influence on solar cell short circuit current.

## References

Anderson PC. 2012. Characteristics of spacecraft charging in low Earth orbit. *J Geophys Res* **117**(A7): 308. <https://doi.org/10.1029/2011JA016875>.

Arimoto S, Sugimura M, Kageyama H, Torimoto T, Kuwabata S. 2008. Development of new techniques for scanning electron microscope observation using ionic liquid. *Electrochim Acta* **53**: 6228–6234. <https://doi.org/10.1016/j.electacta.2008.01.001>.

Aspnes DE, Studna AA. 1983. Dielectric functions and optical parameters of Si, Ge, GaP, GaAs, GaSb, InP, InAs, and InSb from 1.5 to 6.0 eV. *Phys Rev B* **27**: 985–1009. <https://doi.org/10.1103/PhysRevB.27.985>.

Belhaj M, Jbara O, Odof S, Msellak K, Eduard R, Andrianov M. 2006. An anomalous contrast in scanning electron microscopy of insulators: The pseudo-mirror effect. *Scanning* **22**: 352–356. <https://doi.org/10.1002/sca.4950220603>.

Biyikli N, Kimukin I, Butun B, Aytur O, Ozbay E. 2004. ITO-Schottky photodiodes for high-performance detection in the UV–IR spectrum. *Sel Top Quantum Electron IEEE J* **10**: 759–765. <https://doi.org/10.1109/JSTQE.2004.833977>.

Bonin G, Orr N, Zee R, Cain J. 2010. Solar array arcing mitigation for polar low-earth orbit spacecraft. *Proc 24th Annu Conf Small Satell* **9012**: 1. <https://doi.org/10.1109/ACCESS.2019.2927811>.

Cazaux J. 2004. Charging in scanning electron microscopy “from inside and outside”. *Scanning* **26**: 181–203. <https://doi.org/10.1002/sca.4950260406>.

Choi H, Lee J, Cho K, Kwak Y, Cho I, Park Y, Kim Y, Baker DN, Reeves GD, Lee D. 2011. Analysis of GEO spacecraft anomalies: Space weather relationships. *Space Weather* **9**(S06): 001. <https://doi.org/10.1029/2010SW000597>.

Fischer U, Zingsheim H. 1981. Sub-microscopic pattern replication with visible light. *J Vacuum Sci Technol* **19**: 881.

Garrett HB, Whittlesey AC. 2012. *Guide to mitigating spacecraft charging effects*, 1st edn. Wiley. ISBN 9781118186459.

Giessibl FJ, Trapas BM. 1994. Piezoresistive cantilevers utilized for scanning tunneling and scanning force microscope in ultrahigh vacuum. *Rev Sci Instrum* **65**(6): 1923–1929. <https://doi.org/10.1063/1.1145232>.

González E, Domínguez A, Rebello de A, Macedo ME. 2012. Physical and excess properties of eight binary mixtures containing water and ionic liquids. *J Chem Eng Data* **57**: 2165–2176. <https://doi.org/10.1021/je201334p>.

Kim YH, Sachse C, Machala ML, May C, Müller-Meskamp L, Leo K. 2011. Highly conductive PEDOT:PSS electrode with optimized solvent and thermal post-treatment for ITO-free organic solar cells. *Adv Funct Mater* **21**(6): 1076–1081. <https://doi.org/10.1002/adfm.201002290>.

Lu Y, Shao Q, Yue H, Yang F. 2019. A review of the space environment effects on spacecraft in different orbits. *IEEE Access* **7**(93): 473.

Malitson IH. 1965. Interspecimen comparison of the refractive index of fused silica. *J Opt Soc Am* **55**(10): 1205–1209.

Orihuela MF, Somoza AM, Colchero J, Ortuño M, Palacios-Lidón E. 2016. Localized charge imaging with scanning Kelvin probe microscopy. *Nanotechnology* **28**(2): 025703. <https://doi.org/10.1088/1361-6528/28/2/025703>.

Ravula S, Larm NE, Mottaleb MA, Heitz MP, Baker GA. 2019. Vapor pressure mapping of ionic liquids and low-volatility fluids using graded isothermal thermogravimetric analysis. *Chem Eng* **3**: 42. <https://doi.org/10.3390/chemengineering3020042>.

Sadewasser S, Glatzel T. 2012. *Kelvin probe force microscopy: measuring and compensating electrostatic forces*. Springer, Berlin Heidelberg ISBN 978-3-642-22566-6. <https://doi.org/10.1007/978-3-642-22566-6>.

Santos S, Verdaguer A. 2016. Imaging water thin films in ambient conditions using atomic force microscopy. *Materials* **9**: 182. <https://doi.org/10.3390/ma9030182>.

Sarno-Smith LK, Larsen BA, Skoug RM, Liemohn MW, Breneman A, Wygant JR, Thomsen MF. 2016. Spacecraft surface charging within geosynchronous orbit observed by the Van Allen probes. *Space Weather* **14**(2): 151–164. <https://doi.org/10.1002/2015SW001345>.

- Schmid M. 2023. *A simple sputter yield calculator*. <https://www2.iap.tuwien.ac.at/www/surface/sputteryield> [Online; accessed 12-April-2024]
- Shaffner TJ, Veld RDV. 1971. ‘Charging’ effects in the scanning electron microscope. *J Phys E Sci Instrum* **4**(9): 633. <https://doi.org/10.1088/0022-3735/4/9/002>.
- Singh V, Kumar T. 2019. Study of modified PEDOT:PSS for tuning the optical properties of its conductive thin films. *J Sci Adv Mater Dev* **4**(4): 538–543. <https://doi.org/10.1016/j.jsamd.2019.08.009>.
- Tsuda T, Nemoto N, Kawakami K, Mochizuki E, Kishida S, Tajiri T, Kushibiki T, Kuwabata S. 2011. SEM observation of wet biological specimens pretreated with room-temperature ionic liquid. *ChemBioChem* **12**: 2547–2550. <https://doi.org/10.1002/cbic.201100476>.
- Vostrikov AV, Prokofeva EN. 2022. Development of accelerated methods for calculating the pattern of current spreading over the surface of spacecraft. *J Space Weather Space Clim* **12**: 29. <https://doi.org/10.1051/swsc/2022018>.

**Cite this article as:** Wendt M, Dorn F, Lange R, Ludwig R, Berdermann J, et al. 2024. Ionic liquid coating for charge mitigation of solar modules in space: Electron microscopy on insulating nanosphere lithography patterned surfaces. *J. Space Weather Space Clim.* **14**, 18. <https://doi.org/10.1051/swsc/2024019>.